Available online at www.sciencedirect.com

ScienceDirect

journal homepage: www.elsevier.com/locate/he

Enhanced performance for photocatalytic hydrogen evolution using MoS_2/graphene hybrids

Gang-Juan Lee [a], *Yu-Hong Hou* [a], *Chin-Yi Chen* [b], *Chien-Yie Tsay* [b], *Yu-Cheng Chang* [b], *Jing-Heng Chen* [c], *Tzyy-Leng Horng* [d], *Sambandam Anandan* [e], *Jerry J. Wu* [a,*]

[a] *Department of Environmental Engineering and Science, Feng Chia University, Taichung, 407, Taiwan*
[b] *Department of Materials Science and Engineering, Feng Chia University, Taichung, 407, Taiwan*
[c] *Department of Photonics, Feng Chia University, Taichung, 407, Taiwan*
[d] *Department of Applied Mathematics, Feng Chia University, Taichung, 407, Taiwan*
[e] *Department of Chemistry, National Institute of Technology, Trichy, India*

HIGHLIGHTS

- Graphene modified MoS_2 could tune the charge transfer resistance and the photo current as well.
- Formic acid acts as electron donor to capture photogenerated holes to improve hydrogen production.
- $MSG_{0.8}$ has the maximum hydrogen evolution rate of 667.2 μmol h^{-1} g^{-1}.

GRAPHICAL ABSTRACT

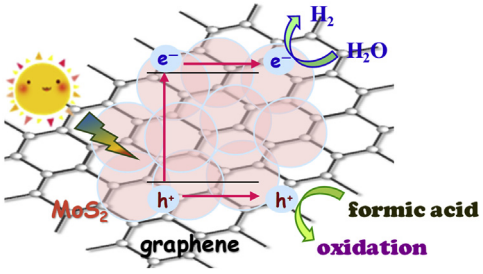

ARTICLE INFO

Article history:
Received 8 February 2020
Received in revised form
27 June 2020
Accepted 1 July 2020
Available online 23 July 2020

Keywords:
MoS_2
Heterostructured photocatalyst
Water splitting
Sacrificial reagent

ABSTRACT

A MoS_2/graphene hybrid (MSG) is synthesized by microwave hydrothermal method. Both of the charge transfer resistance and the photocurrent are tuned in graphene modified MoS_2 by enhancing photocatalytic nature, where the charge transfer resistance significantly decreases from 36,000 Ω–8.49 Ω and the photocurrent promotes from 0.29 mA cm^{-2} to 16.47 mA cm^{-2}. In this article, the result reveals that the appropriate modification of graphene can reach the maximum yield of hydrogen gas. In addition, the appropriate conditions, such as the concentration of 0.32 M formic acid and the MoS_2 photocatalyst with 0.8 wt% graphene ($MSG_{0.8}$) dose of 0.013 g L^{-1}, can complete the outstanding photocatalytic hydrogen evolution, where the hydrogen evolution using $MSG_{0.8}$ composite photocatalyst has the maximum yield of 667.2 μmol h^{-1} g^{-1}.

* *Corresponding author.*
E-mail address: jjwu@mail.fcu.edu.tw (J.J. Wu).
https://doi.org/10.1016/j.ijhydene.2020.07.003

Introduction

Hydrogen involves the characteristics of the clean/renewable energy source, convenient storage, and high energy density. Photocatalytic hydrogen production using semiconductors has been always the potential strategy for the alternative solar fuels [1,2]. All forms of molybdenum disulfide (MoS_2) have a layered structure and three crystalline phases, such as octahedral (tetragonal symmetry, 1T), trigonal prismatic (hexagonal symmetry, 2H), and trigonal prismatic (rhombohedral symmetry, 3R). The 1T phase shows metallic property, while both 2H and 3R phases display semiconductor properties [3–5]. A typical layered structure of MoS_2 could act as a promising photocatalysts for the hydrogen evolution reactions [6–9], because the photocatalytic hydrogen evolution reaction activity was essentially originated from the sulfur edges of MoS_2 photocatalysts [10–12]. However, the number of active sites of MoS_2 is limited to edges, resulting in a poor photocatalytic activity [13]. Therefore, MoS_2 not only needs to enhance the number of active sites and the activity of catalytic sites, but also needs to improve the charge transfer. In this article, we synthesized a MoS_2/graphene hybrid (MSG) to augment the charge transfer of MoS_2. Since graphene displays the excellent electron mobility, it can be a cocatalyst for photocatalytic system to improve the electron (e^-) transfer of MoS_2 [3,7]. Li et al. (2011) [6] synthesized the MoS_2 nanoparticles on reduced graphene oxide (RGO) sheets and demonstrated the excellent hydrogen evolution reaction activity of MoS_2/RGO hybrid material. Zhang et al. (2018) [14] also demonstrated that hybrid MoS_2/graphene catalysts display significantly increased reactivity and stability towards the hydrogen evolution reaction. Gnanasekar al. (2019) [15] showed that vertical MoS_2 nanosheets on graphene structure can perform the rapid charge transfer to improve the performance of electrocatalytic hydrogen evolution. In addition, metal chalcogenide semiconductor is an unstable photocatalyst as photocorrosion is simultaneously induced when the holes (h^+) oxidize the material itself. Therefore, developing efficient photocatalysts for photocatalytic hydrogen production with an efficient sacrificial reagent is of great interest. In this article, two types of sacrificial reagent, such as inorganic and organic solution, were used as the electron donor. The sacrificial reagents would be photo-oxidized prior to the happening of photocorrosion of metal chalcogenide semiconductor, which resulted in improving not only stability, but also photocatalytic activity of metal chalcogenide semiconductor.

According to our previous study, ZnS (metal chalcogenide nanomaterials) has shown the excellent photocatalytic performance via an appropriate modification [16–19]. In view of the above results, the modification of photocatalysts can not only efficiently capture the solar light, but also enhance the charge separation. Therefore, molybdenum disulfide (MoS_2) was chosen in this study as a promising candidate photocatalyst for hydrogen production.

Methods

MoS_2/graphene hybrid photocatalysts

0.1 M $Na_2MoO_4 \cdot 2H_2O$ (sodium molybdenum oxide dehydrate, 98%, Alfa Aesar) and 0.22 M C_2H_5NS (thioacetamide, 99%, Merck) dissolved in the DI water. 0–9.1 wt% multi-layer graphene (Enerage) was put into MoS_2 solution and heated in the microwave reaction system (2450 MHz, 1800 W, MARS 6, CEM). The operating conditions were 450 W, 160 °C, and 20 min. The obtained MoS_2/graphene hybrid powders (0–9.1 wt%) are denoted as MoS_2, $MSG_{0.6}$, $MSG_{0.8}$, $MSG_{1.0}$, $MSG_{1.2}$, $MSG_{2.4}$, $MSG_{4.8}$, and $MSG_{9.1}$, respectively.

Characterization tools

The morphologies were characterized by JEOL JEM-1400, JEOL JSM-7800F model, and JEOL JEM-2010 model. XRD patterns were examined by Rigaku Ultima III diffractometer (Japan) from 10° to 80°. XPS, particle size distribution, BET, UV–visible diffuse reflectance spectra, and PL properties were recorded using Physical Electronics PHI 5600 XPS, Shimadzu SALD-2300, Micrometrics ASAP-2020, Shimadzu UV-2600 spectrophotometer, and Shimadzu RF-3501 equipment, respectively. The flat-band potential, charge-transfer resistance, and photo current of the MoS_2/graphene hybrid photocatalysts were analyzed by Potentiostat/Galvanostat instrument of Metrohm Autolab [17].

Hydrogen evolution

The photocatalytic hydrogen evolution was conducted using 100 mL solution containing various sacrificial reagents (0.1 M), such as sodium sulfide ($Na_2S \cdot 9H_2O$, 98%, Acros), sodium sulfite (Na_2SO_3, 99%, anreac Quimica SAU), sodium sulfate (Na_2SO_4, 99%, Merck), methanol (CH_3OH, 99.9%, Merck), ethanol (C_2H_5OH, EtOH, 95%, FERAK), formic acid (HCOOH, 98%–100%, Merck), lactic acid ($C_3H_6O_3$, 85%, TEDIA), and EDTA (ethylenediaminetetraacetic acid, $C_{10}H_{16}N_2O_8$, 96%, SHOWA), and the MoS_2/graphene hybrid photocatalysts at the dosage 0–0.15 g L^{-1}. Subsequently, argon was used to purge the solution for 10 min to avoid any interference, such as nitrogen and oxygen. The reactor was irradiated with a 350 W Xenon light (KIT-XENON-ADJ350W) for 6 h and the production was determined by GC/TCD (GC-2014, SHIMADZU).

Results and discussion

Characterization of MoS_2/graphene hybrid photocatalysts

The effect of irradiation time and reaction temperature by microwave dynamics on the constitution of MoS_2 nanostructure was shown in Fig. 1 and Fig. 2, respectively. As the time prolonged from 10 min to 1 h, the particle size of MoS_2

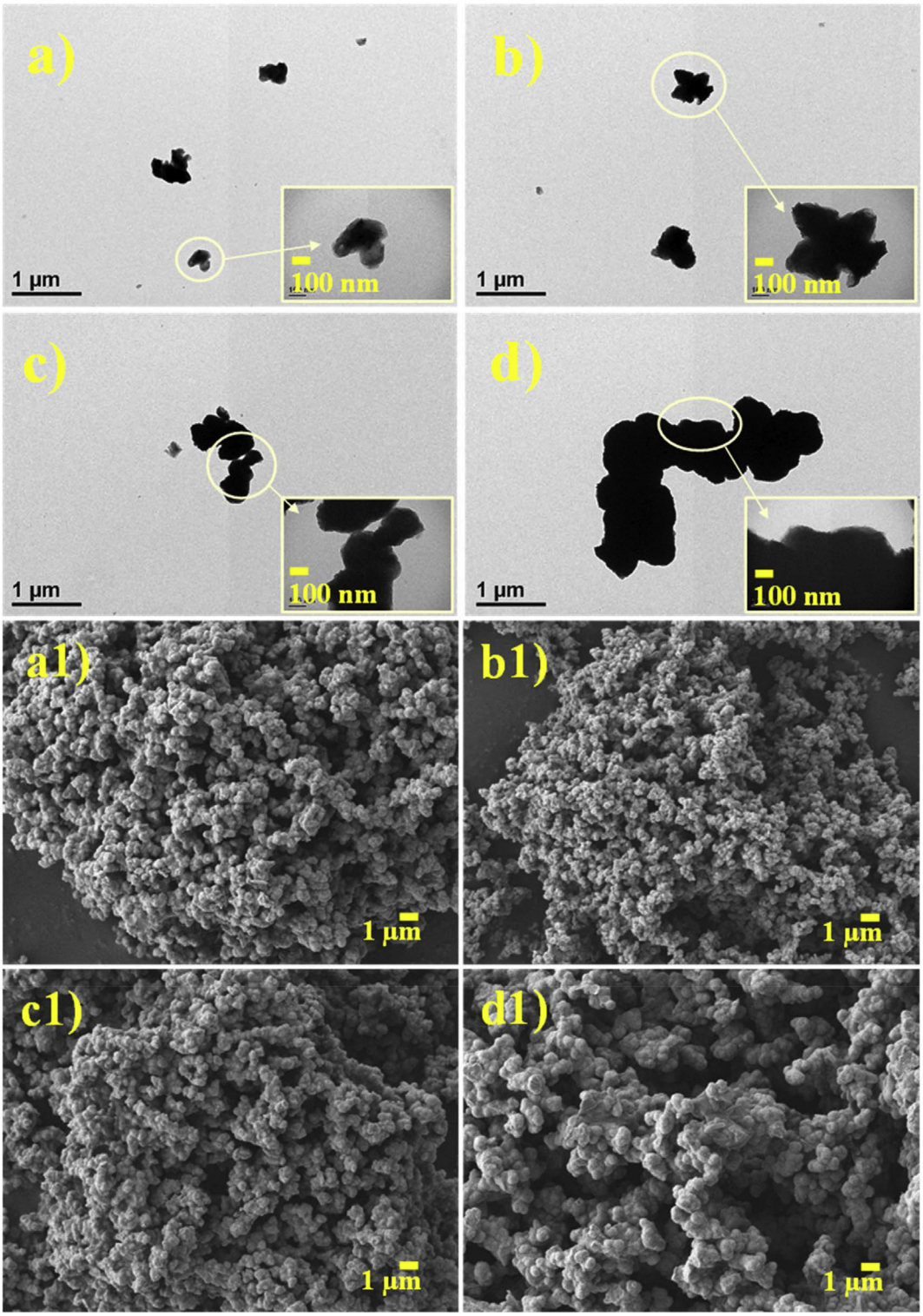

Fig. 1 – TEM and FESEM images of as-synthesized MoS_2 photocatalysts with different microwave irradiation times (a) 160 °C/10 min, (b) 160 °C/20 min, (c) 160 °C/30 min, (d) 160 °C/60 min.

gradually became larger, even agglomerated powders were formed because surface molecules (Mo and S ions) move from one crystal to another and the larger crystals form as the reaction time prolonged according to the Ostwald ripening process and oriented attachment mechanism, where nanoparticles with common crystallographic orientations directly combine together to form larger ones. Fig. 2a and b display the morphologies of MoS_2 from 160 °C to 180 °C, where the diameter of the MoS_2 micro-ball significantly increases. From Fig. 2a1 image of MoS_2 micro-ball, the MoS_2 micro-ball was the wool-like surface made up of sheets. Both samples indicate a broadened feature in XRD patterns due to low crystallinity,

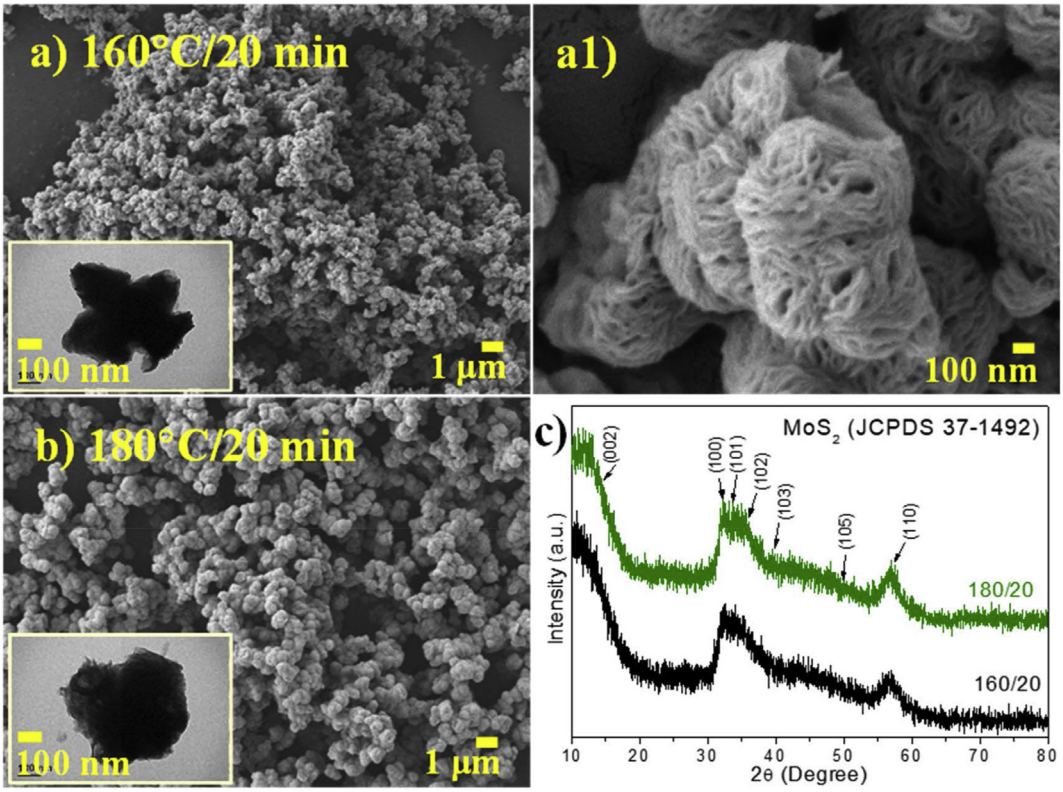

Fig. 2 – FESEM images, and XRD patterns of as-synthesized MoS_2 photocatalysts with different reaction temperature. Insets show the TEM images for the corresponding samples.

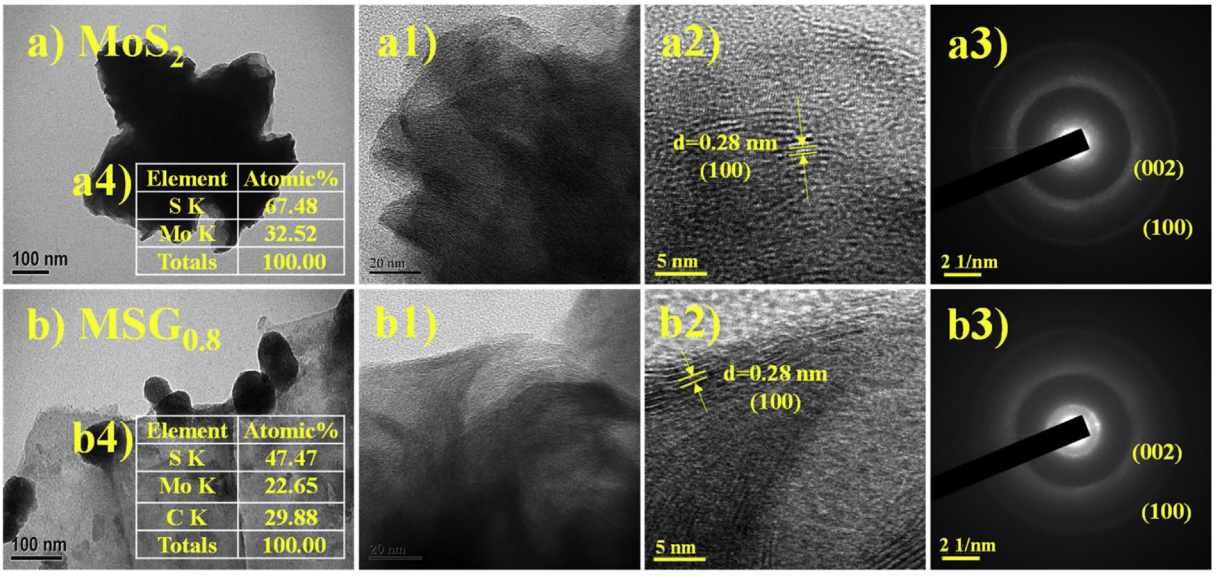

Fig. 3 – (a)–(b) TEM image, (a1)–(b1) magnified HRTEM image, (a2)–(b2) lattice fringes, (a3)–(b3) corresponding SAED pattern, and (a4)–(b4) EDX of MoS_2 and $MSG_{0.8}$ photocatalysts.

whereas all the peaks match the hexagonal structure of MoS_2 (2H–MoS_2) (JCPDS Card No. 37-1492) as shown in Fig. 2c. The morphology of the as-prepared MoS_2 was further characterized by HR-TEM as shown in Fig. 3a. Fig. 3a2 reveals the crystalline nature of MoS_2 and well-resolved lattice fringes with an interplanar (100) distance of MoS_2 is measured as 0.28 nm. The corresponding selected area electron diffraction (SAED) pattern exhibits rings as shown in Fig. 3a3, which indicates as-synthesized MoS_2 is of polycrystalline structure. In addition, EDX image and its ratio clearly show that the purity of MoS_2 is approximately to 100% (1:2 M ratio) as shown in Fig. 3a4. Therefore, the experimental condition at 160 °C for

20 min was selected as the better parameter to synthesize MoS_2/graphene hybrid materials.

As the graphene weight ratio was added from 0.6 wt% to 2.4 wt%, the MoS_2 particles (green mark) could grow on graphene (pink mark) surface (Fig. 4a–e). Increasing the weight ratio of graphene until 4.8 wt%, a smooth surface of graphene was obtained (Fig. 4f). Since the density of graphene is much smaller than that of MoS_2, the concentration of 4.8 wt% graphene would be significantly larger than that of MoS_2 and tend to restack and agglomerate as shown in Fig. 4f1, which matches well with the result of D_{50} as shown in Table 1. Therefore, the presence of excess graphene cannot produce MoS_2 on the surface of graphene. In addition, Fig. 5 exhibits the XRD patterns of MoS_2/graphene hybrid photocatalysts with different amounts of graphene. As the graphene is added up to 1.0 wt%, the diffraction peaks become hexagonal phase of graphene (JCPDS Card No. 75-1621) and the peaks of MoS_2 disappear due to the relative smaller density of graphene with high volume distribution around the composite. Although it doesn't show the diffraction peaks of MoS_2 with graphene weight ratio from 1.0 wt% to 2.4 wt%, the MoS_2 particles can substantially grow on graphene surface from TEM observation (Fig. 4). Furthermore, the HR-TEM characterization of MoS_2 with 0.8 wt% graphene was also further analyzed in Fig. 3b. Fig. 3b2 reveals the crystalline nature of $MSG_{0.8}$ and well-resolved lattice fringes with an interplanar (100) distance of MoS_2 is measured as 0.28 nm. The SAED pattern exhibits rings as shown in Fig. 3b3, which indicate $MSG_{0.8}$ is also of polycrystalline structure. The EDS spectrum of MoS_2/graphene composite reveals the presence of C, Mo, and S elements. The measured Mo/S atomic ratio is around 0.47, which is consistent with the stoichiometric ratio of MoS_2 (1:2) as shown in Fig. 3b4. Therefore, MoS_2/graphene hybrid photocatalysts (0–1.2 wt%) was employed to do the photocatalytic hydrogen evolution.

The chemical states of the Mo and S were recorded by XPS as shown in Fig. 6. The C1s core level peak is used as energy reference located in 284.4 eV as shown in Fig. 6a. The binding

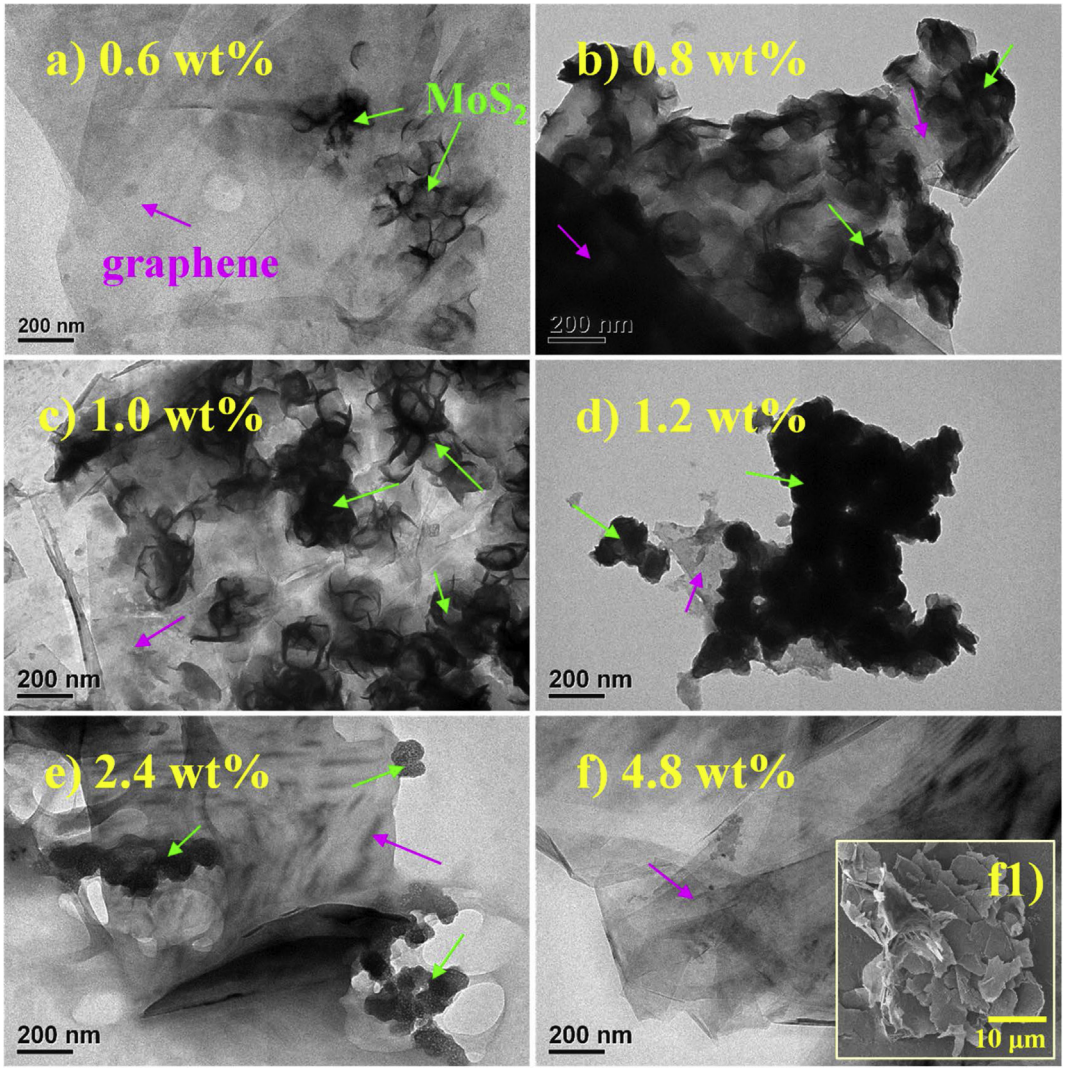

Fig. 4 – TEM and FESEM images of as-synthesized MoS_2/graphene hybrid photocatalysts with different amounts of graphene. (green mark: MoS_2, pink mark: graphene). (For interpretation of the references to color in this figure legend, the reader is referred to the Web version of this article.)

Table 1 – Summary of particle size distribution, BET, charge transfer resistance, and photo current of MoS_2/graphene hybrid photocatalysts.

photocatalyst	MoS_2	$MSG_{0.6}$	$MSG_{0.8}$	$MSG_{1.0}$	$MSG_{1.2}$
D_{50} (μm)[a]	2.01	8.89	13.30	15.53	17.36
BET ($m^2\ g^{-1}$)	2.31	17.62	39.84	11.41	6.66
R_{ct} (Ω)[b]	36,000	1510	8.49	12.2	18.7
Photocurrent (mA cm^{-2})	0.29	3.50	16.47	1.43	9.09

[a] Particle size distribution D_{50} is known as the median diameter or the medium value of the particle size distribution, it is the value of the particle diameter at 50% in the cumulative distribution.
[b] R_{ct} is the charge transfer resistance, the parameters obtained from the fitting of the equivalent electric circuit to the experimental impedance data obtained for different amount of graphene.

energy of Mo $3d_{5/2}$ and Mo $3d_{3/2}$ are displayed at 228.8 eV and 232.9 eV (Fig. 6b), pertaining to the Mo^{4+} oxidation state [20–22]. The peaks are found to be slightly shifted to lower binding energies after the addition of graphene, which is the indication of partial charge transfer from the MoS_2 to graphene or the additional loss of S in the surroundings of sulfur vacancies. Therefore, the peak of doublet corresponds to the presence of inter-coordinated Mo in MoS_{2-x} and sulfur vacancies in MoS_2 layers. The results can match well with valence band XPS spectra in Fig. 6c. The valence band maximum (VBM) position of MoS_2 is showed at 0.66 eV and it shifts to 0.58 eV after the modification of graphene, which reveals the presence of the sulfur defects on the MoS_2/graphene structure. Therefore, the VBM shifts close to the Fermi level, resulting in a reduced band gap [23]. Furthermore, the peak at 235.9 eV corresponds to the Mo^{6+} of MoO_3. The Mo^{6+} peak indicates that some oxygen is incorporated in the MoS_2 infrastructure. Sulfur atom peak was exhibited at 226.0 eV and S^{2-} peaks were noted at 161.6 eV and 162.8 eV due to S $2p_{3/2}$ and S $2p_{1/2}$, respectively. Additionally, the peak at 163.8 eV implies the existence of bridging S_2^{2-} or apical S^{2-} as shown in Fig. 6d [24].

Hydrogen evolution

The activities of MoS_2/graphene hybrid materials were evaluated for the photocatalytic hydrogen evolution via simulated solar light. The major parameters, such as the pH value of solution, the dosages of $MSG_{0.8}$, the various types of sacrificial reagents, the concentration of formic acid, and the types of MoS_2/graphene hybrid photocatalysts, were evaluated as below to investigate the evolution efficiency of solar fuels as generated.

Solution pH value

Fig. 7 reveals the effect on hydrogen production of 0.15 g L^{-1} $MSG_{0.8}$ upon the addition of 0.1 M Na_2S solution at different pH values (such as 3, 7, 9, and 11.7). The highest activity of hydrogen evolution (17.6 μmol $g^{-1}\ h^{-1}$) was achieved at pH 7. According to the references, the key factor for the half reaction of the photocatalysis is the nature of active ions [25–27]. The prevailing ion is the proton in acidic solution. However, $MSG_{0.8}$ has more positive surface charges at lower pH values due to higher zero point charge of $MSG_{0.8}$ catalyst (pH_{zpc} = 10.1). Therefore, there is the electrostatic repulsion force between $MSG_{0.8}$ and H^+ ions, resulting in a poor hydrogen evolution reaction activity as shown in the reaction (1) of Fig. 7. In contrast, hydroxide ion appears to be the dominant ion in alkaline solution. Since there are more OH^- in the Na_2S solution at pH 11.7, the reaction would prefer to the reverse reaction. Therefore, it leads to an obviously decreased H_2 evolution as shown in the reaction (2) of Fig. 7. On the basis of the above results, pH 7 could give the maximum hydrogen production efficiency compared to the other pHs.

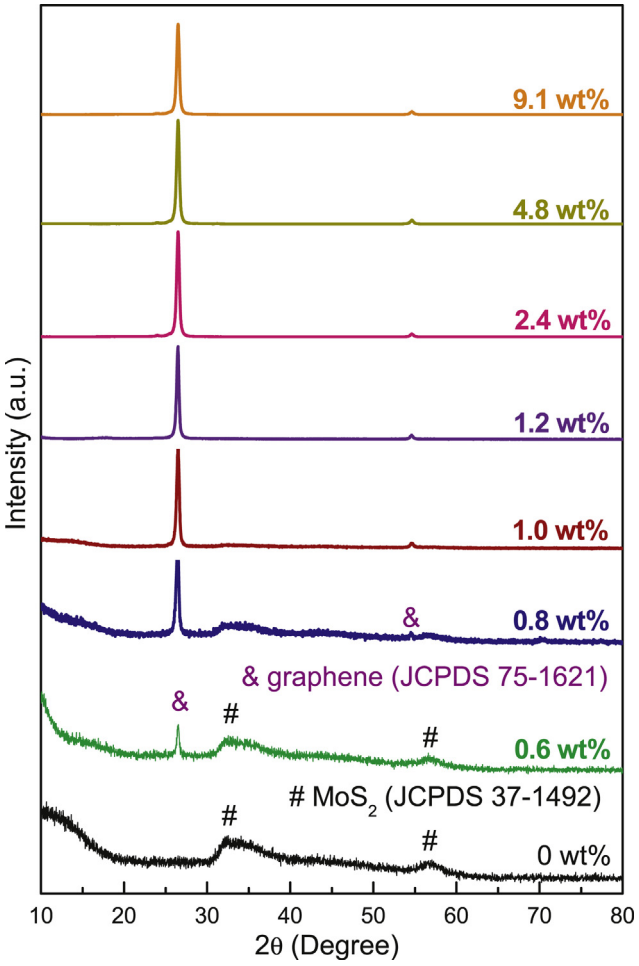

Fig. 5 – XRD patterns of as-synthesized MoS_2/graphene hybrid photocatalysts with different amounts of graphene.

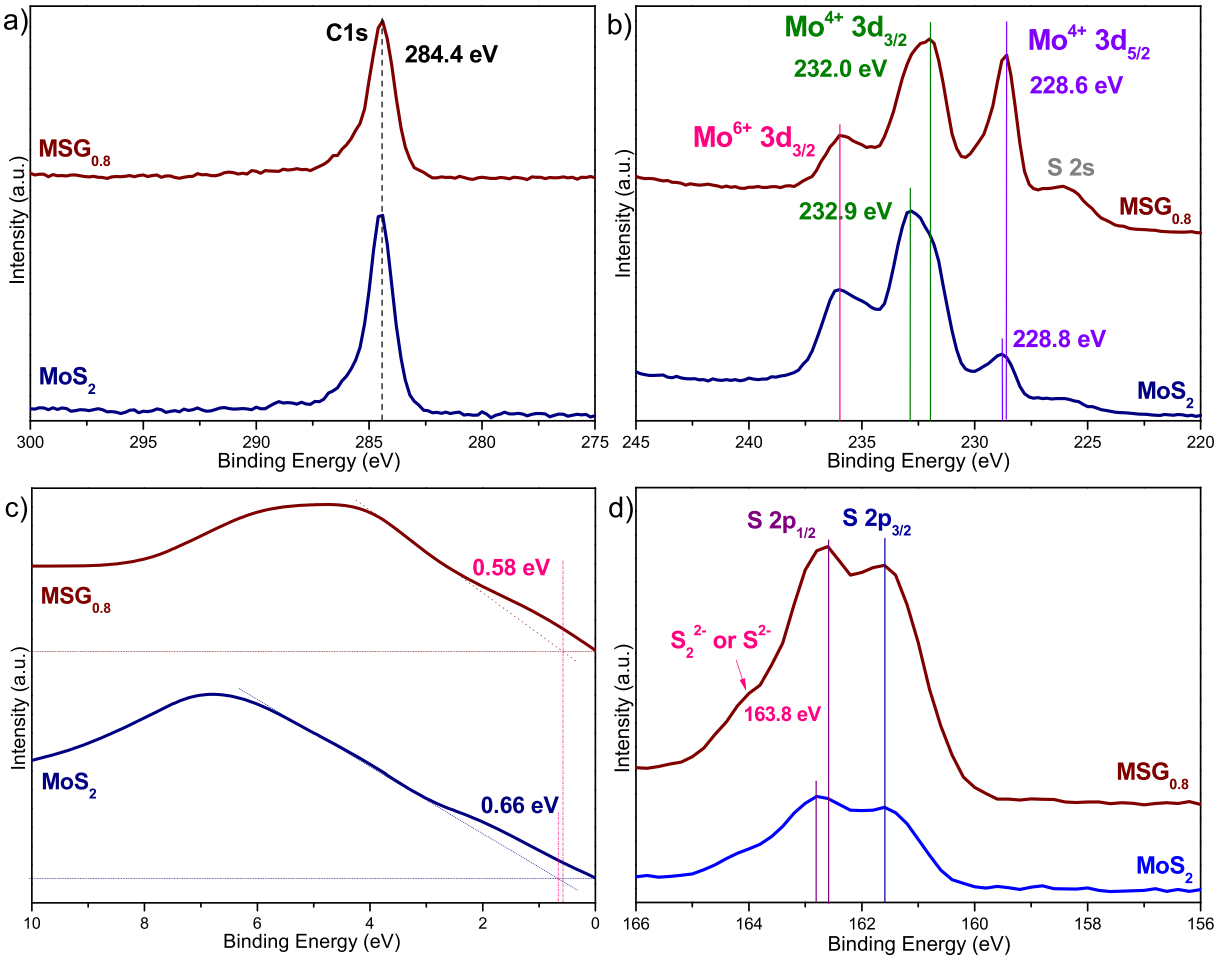

Fig. 6 – (a) C1s, (b) Mo3d, (c) valence band, and (d) S2p XPS spectra for MoS_2 and $MSG_{0.8}$ samples.

Dosage of $MSG_{0.8}$

We selected various amount of $MSG_{0.8}$ from 0.006 g L^{-1} to 0.15 g L^{-1} to evaluate photocatalytic hydrogen evolution by photocatalyst dosage change. The highest activity of hydrogen evolution (264.9 μmol g^{-1} h^{-1}) is implemented at 0.013 g L^{-1} (Fig. 8). Moreover, with increasing amount of $MSG_{0.8}$ photocatalyst, the hydrogen evolution activity decreased. The reason is that more powders would induce the aggregation of particles and reduce the surface area of the reaction, resulting

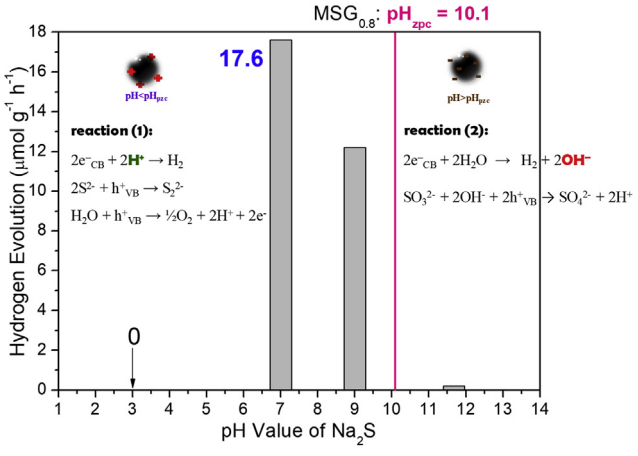

Fig. 7 – Influence of the pH value of Na_2S to hydrogen evolution from an aqueous solution containing 0.1 M Na_2S and 0.15 g L^{-1} of $MSG_{0.8}$ photocatalyst.

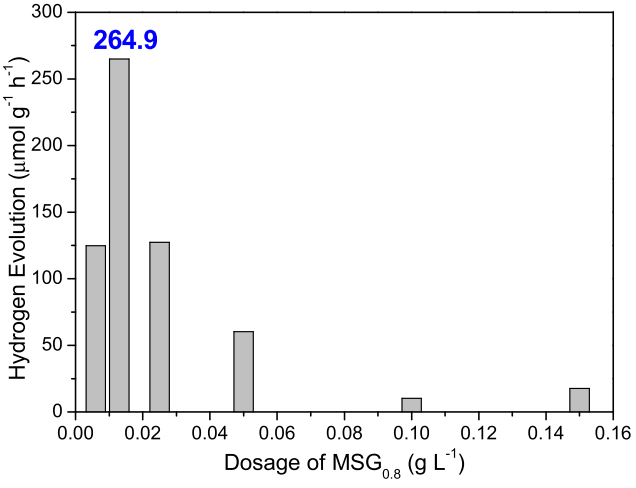

Fig. 8 – Effect of the dosage of $MSG_{0.8}$ photocatalyst on hydrogen evolution rate for an aqueous solution containing 0.1 M Na_2S at pH 7.

in the lower photocatalytic activity. The other reason is due to the scattering of light in such a high turbid reaction system. Therefore, the appropriate dosage of photocatalyst could exhibit more outstanding photocatalytic performance.

Types of sacrificial reagents

Sacrificial reagents could play a prominent role in the photocatalytic reaction system because it can act an electron donor to maintain the stability of photocatalyst. Therefore, we chose two types of sacrificial reagents, such as inorganic and organic solution, to evaluate the photocatalytic hydrogen evolution efficiency of $MSG_{0.8}$ as shown in Fig. 9a. For inorganic solution, using the Na_2S solution, it can reach the higher H_2 evolution efficiency (264.9 μmol g^{-1} h^{-1}) due to the redox potentials of Na_2S (Fig. 9b). As the redox potential of sacrificial reagent, Na_2S is more positive than conduction band and more negative than valence band of $MSG_{0.8}$ photocatalyst, thus it can react with the h^+ and inhibit the recombination of e^-/h^+ [28]. The other reason is that Na_2S is more unstable than $MSG_{0.8}$ material, leading to more tendency to oxidize Na_2S by electron holes. Therefore, it could reduce the photocorrosion of $MSG_{0.8}$ and enhance photocatalytic stability. Meanwhile, using the formic acid solution can produce the maximum hydrogen production rate (280.5 μmol g^{-1} h^{-1}) (Fig. 9b). The factors that influence photocatalytic reaction are oxidation potential and dielectric constant of sacrificial reagent [28]. Therefore, formic acid with lower oxidation potentials (1.02 eV) and higher dielectric constant (58.5) would allow for higher photocatalytic H_2 evolution rate (Fig. 9c).

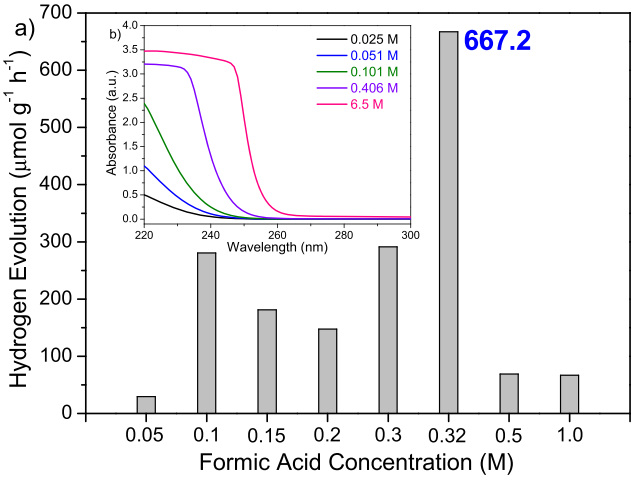

Fig. 10 – (a) Effect of the concentration of formic acid to hydrogen evolution rate from an aqueous solution containing 0.013 g L^{-1} of $MSG_{0.8}$ photocatalyst. (b) UV–vis absorption spectra of formic acid with different concentrations.

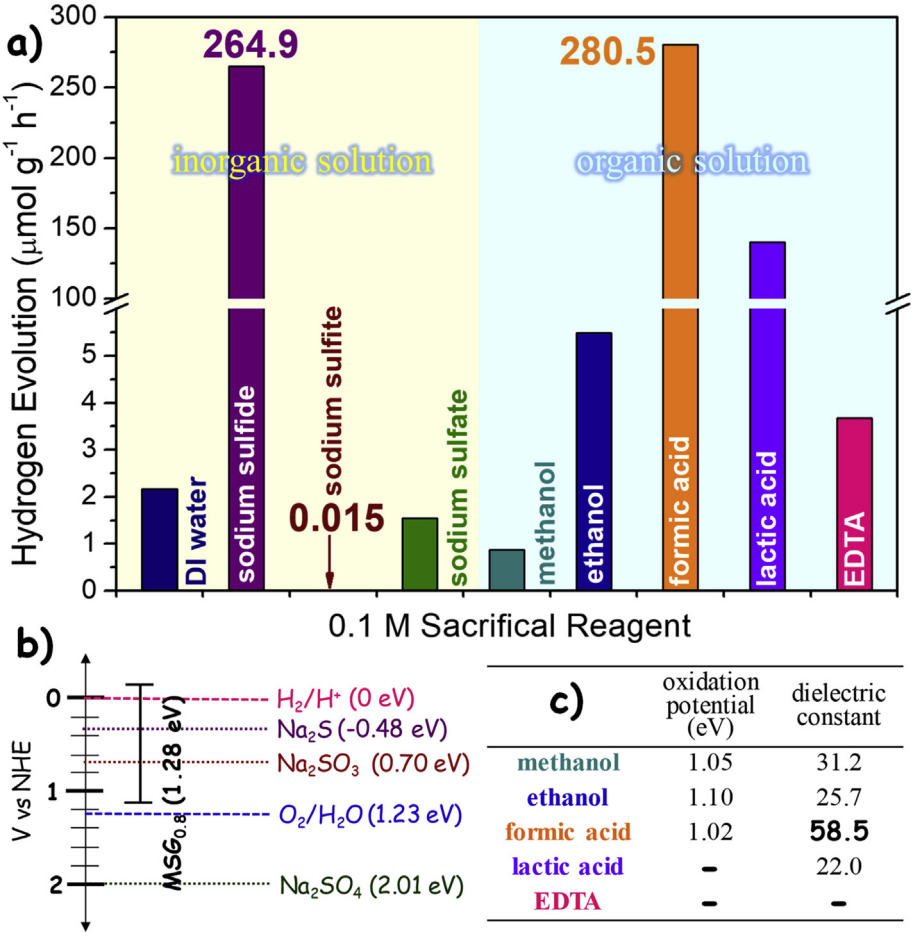

c)	oxidation potential (eV)	dielectric constant
methanol	1.05	31.2
ethanol	1.10	25.7
formic acid	1.02	**58.5**
lactic acid	-	22.0
EDTA	-	-

Fig. 9 – (a) Comparison of photocatalytic hydrogen evolution rate over $MSG_{0.8}$ photocatalyst using various sacrificial reagents. (b) The redox potentials of sacrificial reagents. (c) Oxidation potential and dielectric constant of organic solution.

Concentration of formic acid

The appropriate concentration of formic acid (0.32 M) could reach the maximum H_2 production rate (667.2 μmol g^{-1} h^{-1}) as shown in Fig. 10a as formic acid acts as electron donor to capture photogenerated holes to improve hydrogen reduction performance. However, a further increase in the concentration of formic acid can lead to a significant decrease in hydrogen evolution rates. Fig. 10b shows the UV–Vis absorption spectra of formic acid with various concentrations, which can be seen that excess formic acid can absorb the simulated sunlight, thus the light harvesting efficiency of photocatalyst reduces, resulting in a lower hydrogen evolution rate.

Types of MoS_2/graphene hybrid photocatalysts

Based on the above results, 0.32 M formic acid and 0.013 g L^{-1} photocatalyst were chosen to conduct the photocatalytic water splitting experiments. Fig. 11a shows the photocatalytic H_2 production efficiencies of MoS_2/graphene hybrid materials with different amounts of graphene. It can be seen that $MSG_{0.8}$ photocatalyst could achieve the maximum hydrogen evolution rate at 667.2 μmol g^{-1} h^{-1}. Meanwhile, we analyzed the physical and chemical characterization of MoS_2/graphene hybrid materials to support the results. UV–Vis absorption of pristine MoS_2 and MoS_2/graphene hybrid materials are demonstrated in Fig. 11c. The calculated band gap using the Tauc's relation decreases significantly from 2.41 to 1.28 eV upon modifying graphene. At the same time, we measured the flat band potentials (Fig. 11d) to calculate the conduction band (CB) and valence band (VB) edge positions of the as-synthesized samples as shown in Fig. 11b [17]. For Fig. 11b, we could know that MoS_2/graphene hybrid photocatalysts possess the suitable band gap energy and the appropriate conduction band edge positions to capture the light and reach the conversion from hydrogen ion to hydrogen.

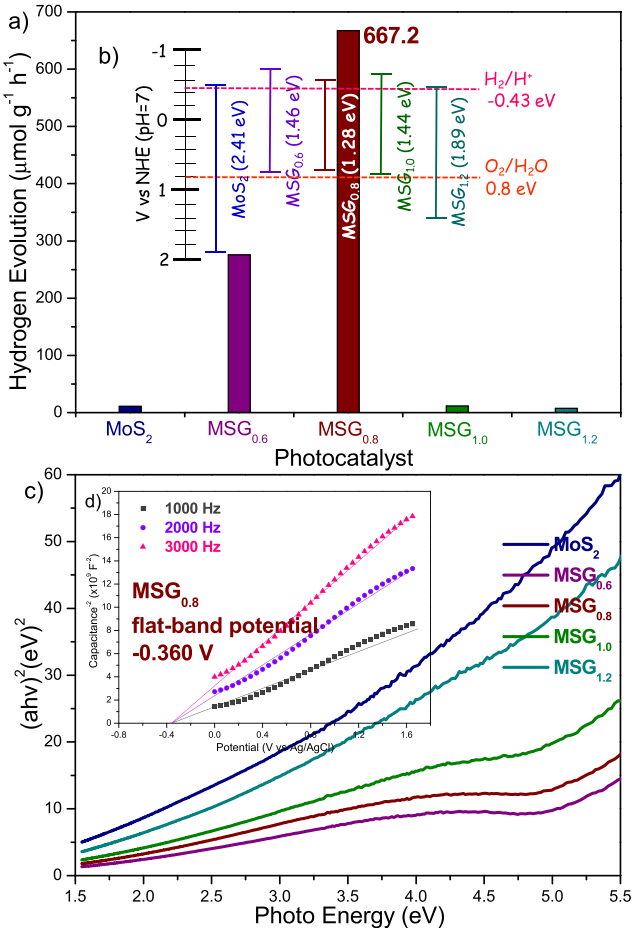

Fig. 11 – (a) photocatalytic hydrogen evolution activities. (b) Energy-level diagram showing the CB and VB edge positions. (c) Band gap plot of as-synthesized MoS_2/graphene hybrid photocatalysts with different amounts of graphene. (d) Mott-Schottky plots for $MSG_{0.8}$ photocatalysts.

Moreover, the porous nature of the as-prepared products was further confirmed by the measurement of pore-size distribution as shown in Table 1 and Fig. 12a. These isotherms display the type IV isotherms with hysteresis loops according to the IUPAC classification, which indicates the presence of mesopores. The result revealed that the appropriate addition of graphene could increase the BET of the samples to a certain degree from 2.31 m^2 g^{-1} to 39.84 m^2 g^{-1}. The MoS_2/graphene composites provide more surface area by increasing the weight ratio of graphene. However, as the presence of excess graphene (>1.0 wt%), graphene sheets gradually stacked and agglomerated, leading to a smaller surface area. Therefore, the maximum surface area of $MSG_{0.8}$ photocatalyst was recognized to provide more active sites for redox reaction. We also analyzed the charge transfer resistance of the as-synthesized MoS_2/graphene hybrid materials to further investigate the electrochemical impedance characteristics. The Nyquist plots and the simulation values R_{ct} of the as-synthesized MoS_2/graphene hybrid materials are demonstrated in Table 1 and Fig. 12b. The resistances are significantly reduced using the graphene from 36,000 Ω–8.49 Ω, whereas the relatively high resistance in the case of pristine MoS_2 without graphene is exhibited. Thus, a smaller charge transfer resistance would enhance the charge transfer, which resulted in the effective charge separation. Fig. 12c shows the linear sweep voltammetry scans of the as-synthesized MoS_2/graphene hybrid materials under UV light irradiation. $MSG_{0.8}$ photocatalyst displayed the maximum photocurrent density, 16.47 mA cm^{-2} at 0.3 V. A higher photocurrent density exhibits that the photons absorbed by photocatalyst can generate the photoexcited carriers efficiently. Since the S–Mo–S layers of MoS_2 structures possess an abundance of exposed edges stacked onto graphene, they should provide significant enhancement of the electron transfer in the MoS_2/graphene hybrid materials. Therefore, $MSG_{0.8}$ photocatalyst has the highest photocatalytic activity. Photoluminescence spectra of the synthesized samples are shown in Fig. 12d. It is observed that PL intensity of pristine MoS_2 sample is higher than that of MoS_2/graphene hybrid materials. The MoS_2/graphene hybrid materials gave an emission peak at 362 nm. As the graphene concentration increases, the intensity of PL emission of MoS_2/graphene hybrid materials pronounced decreases. The peaks at 450–500 nm can attribute to S vacancies and these S vacancies lead to the enhancement of blue-indigo-violet emission. The result matches well with XPS analysis (Fig. 6c). According to literature, the unsymmetric nature of the PL spectra with multiple peaks is due to the various native defect levels that may be present in the prepared products [29]. On the basis of aforementioned discussion, $MSG_{0.8}$

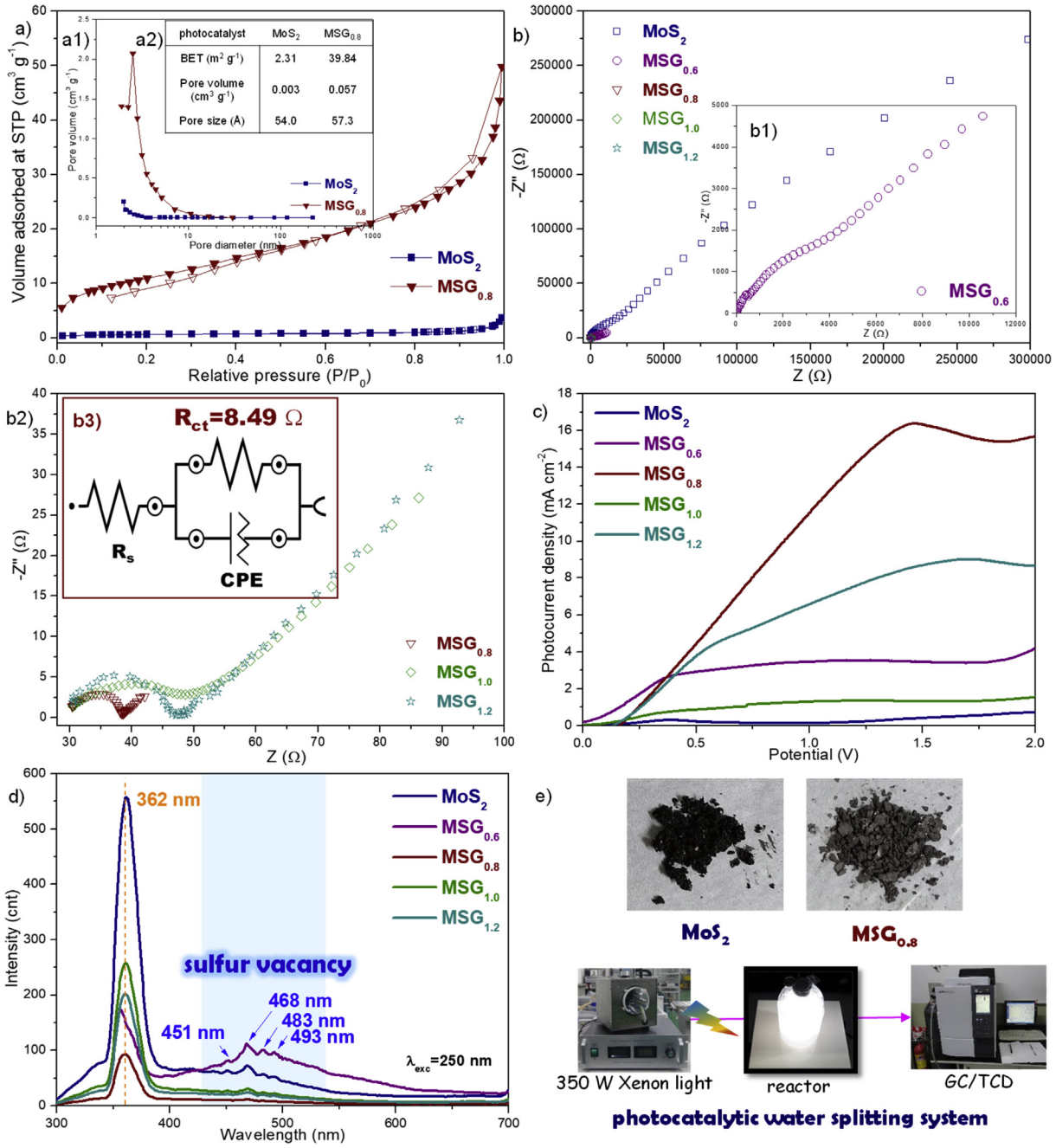

Fig. 12 – (a) Nitrogen adsorption–desorption curve and (a1) Barrett–Joyner–Halenda (BJH) pore diameter distribution of MoS_2 and $MSG_{0.8}$. (b) Nyquist plots for all photocatalysts, (b1) Enlarged Nyquist plot for $MSG_{0.8}$, (b2) Nyquist plots for $MSG_{0.8}$, $MSG_{1.0}$, and $MSG_{1.2}$ photocatalysts (b3) Equivalent electric circuits of $MSG_{0.8}$ photocatalysts, where R_s: a resistor due to electrolyte solution resistance, R_{ct}: charge transfer resistance, and CPE: a capacitor due to double-layer capacitance. (c) Photocurrent density-potential curves. (d) PL spectra of as-synthesized MoS_2/graphene hybrid photocatalysts with different amounts of graphene. (e) Digital camera images for the corresponding samples and photo of the system setup for the hydrogen evolution.

photocatalyst has an outstanding hydrogen production efficiency due to the maximum specific surface area, the minimum charge transfer resistance, the maximum photocurrent density, and the lower PL intensity as shown in Table 1, and Fig. 12. Moreover, we provide the digital camera images for the corresponding samples, and photo of the system setup for the hydrogen evolution as shown in Fig. 12e.

Conclusion

In summary, a MoS_2/graphene hybrid was successfully synthesized by microwave assisted hydrothermal method. Graphene modified MoS_2 could tune the charge transfer resistance and the photocurrent as well. Oxidation potential, dielectric constant, and concentration of sacrificial reagent

can also influence the photocatalytic activity. The appropriate concentration using 0.32 M formic acid and the $MSG_{0.8}$ photocatalyst dosage of 0.013 g L^{-1} could achieve the maximum hydrogen evolution rate at 667.2 μmol g^{-1} h^{-1}.

Declaration of competing interest

The authors declare that they have no known competing financial interests or personal relationships that could have appeared to influence the work reported in this paper.

Acknowledgements

The authors would be grateful to the financial support of Ministry of Science and Technology (MOST) in Taiwan under the contract number of MOST-107-2221-E-035-001-MY3 and MOST-108-2218-E-035-010.

REFERENCES

[1] Lee GJ, Wu JJ. Recent developments in ZnS photocatalysts from synthesis to photocatalytic applications - a review. Powder Technol 2017;318:8–22.
[2] Wu JJ, Lee GJ. Advanced nanomaterials for water splitting and hydrogen generation. Nanomaterials for green energy. Elsevier; 2018. p. 145–67.
[3] Toh RJ, Sofer Z, Luxa J, Sedmidubsky D, Pumera M. 3R phase of MoS_2 and WS_2 outperforms the corresponding 2H phase for hydrogen evolution. Chem Commun 2017;53:3054–7.
[4] Xiong P, Ma R, Sakai N, Nurdiwijayanto L, Sasaki T. Unilamellar metallic MoS_2/graphene superlattice for efficient sodium storage and hydrogen evolution. ACS Energy Lett 2018;3(4):997–1005.
[5] Guo J, Li F, Sun Y, Zhang X, Tang L. Oxygen-incorporated MoS_2 ultrathin nanosheets grown on graphene for efficient electrochemical hydrogen evolution. J Power Sources 2015;291:195–200.
[6] Li Y, Wang H, Xie L, Liang Y, Hong G, Dai H. MoS_2 nanoparticles grown on graphene: an advanced catalyst for the hydrogen evolution reaction. J Am Chem Soc 2011;133:7296–9.
[7] Chang K, Mei Z, Wang T, Kang Q, Ouyang S, Ye J. MoS_2/graphene cocatalyst for efficient photocatalytic H_2 evolution under visible light irradiation. ACS Nano 2014;8:7078–87.
[8] Hu WH, Han GQ, Dai FN, Liu YR, Shang X, Dong B, Chai YM, Liu CG. Effect of pH on the growth of MoS_2 (002) plane and electrocatalytic activity for HER. Int J Hydrogen Energy 2016;41:294–9.
[9] Han GQ, Shang X, Lu SS, Dong B, Li X, Liu YR, Hu WH, Zeng JB, Chia YM, Liu CG. Electrodeposited MoS_x films assisted by liquid crystal template with ultrahigh electrocatalytic activity for hydrogen evolution reaction. Int J Hydrogen Energy 2017;42:5132–8.
[10] Hinnemann B, Moses PG, Bonde J, Jørgensen KP, Nielsen JH, Horch S, Chorkendorff I, Nørskov JK. Biomimetic hydrogen evolution: MoS_2 nanoparticles as catalyst for hydrogen evolution. J Am Chem Soc 2005;127:5308–9.
[11] Jaramillo TF, Jørgensen KP, Bonde J, Nielsen JH, Horch S, Chorkendorff I. Identification of active edge sites for electrochemical H_2 evolution from MoS_2 nanocatalysts. Science 2007;317:100–2.
[12] Bonde J, Moses PG, Jaramillo TF, Nørskov JK, Chorkendorff I. Hydrogen evolution on nano-particulate transition metal sulfides. Faraday Discuss 2008;140:219–31.
[13] Voiry D, Salehi M, Silva R, Fujita T, Chen M, Asefa T, Shenoy VB, Eda G, Chhowalla M. Conducting MoS_2 nanosheets as catalysts for hydrogen evolution Reaction. Nano Lett 2013;13:6222–7.
[14] Zhang X, Zhang M, Tian Y, You J, Yang C, Su J, Li Y, Gao Y, Gu H. In situ synthesis of MoS_2/graphene nanosheets as free-standing and flexible electrode paper for high efficiency hydrogen evolution reaction. RSC Adv 2018;8:10698–705.
[15] Gnanasekar P, Periyanagounder D, Kulandaivel J. Vertically aligned MoS_2 nanosheets on graphene for highly stable electrocatalytic hydrogen evolution reactions. Nanoscale 2019;11(5):2439–46.
[16] Lee GJ, Anandan S, Masten SJ, Wu JJ. Sonochemical synthesis of hollow copper doped zinc sulfide nanostructures: optical and catalytic properties for visible light assisted photosplitting of water. Ind Eng Chem Res 2014;53(21):8766–72.
[17] Lee GJ, Anandan S, Masten SJ, Wu JJ. Photocatalytic hydrogen evolution from water splitting using Cu doped ZnS microspheres under visible light irradiation. Renew Energy 2016;89:18–26.
[18] Lee GJ, Chen HC, Wu JJ. (In, Cu) Co-doped ZnS nanoparticles for photoelectrochemical hydrogen production. Int J Hydrogen Energy 2019;44(1):110–7.
[19] Lee GJ, Chen HC, Wu JJ. Enhancing the photocatalytic hydrogen evolution of copper doped zinc sulfide nanoballs through surfactants modification. Int J Hydrogen Energy 2019;44:30563–73.
[20] Wu Z, Li B, Xue Y, Li J, Zhang Y, Gao F. Fabrication of defect-rich MoS_2 ultrathin nanosheets for application in lithium-ion batteries and supercapacitors. J Mater Chem 2015;3(38):19445–54.
[21] Ho YT, Ma CH, Luong TT, Wei LL, Yen TC, Hsu WT, Chang EY. Layered MoS_2 grown on c-sapphire by pulsed laser deposition. Phys Status Solidi RRL 2015;9(3):187–91.
[22] Li X, Feng Z, Zai J, Ma ZF, Qian X. Incorporation of Co into MoS_2/graphene nanocomposites: one effective way to enhance the cycling stability of Li/Na storage. J Power Sources 2018;373:103–9.
[23] Park Y, Li N, Lee G, Kim KS, Kim KJ, Hong SC, Han SW. Sulfur-vacancy-dependent geometric and electronic structure of bismuth adsorbed on MoS_2. Phys Rev B 2018;97:115307.
[24] Shang X, Hu WH, Li X, Dong B, Liu YR, Han GQ, Chai YM, Liu CG. Oriented stacking along vertical (002) planes of MoS_2: a novel assembling style to enhance activity for hydrogen evolution. Electrochim Acta 2017;224:25–31.
[25] Opu MS. Effect of operating parameters on performance of alkaline water electrolysis. Int J Therm Environ Eng 2015;9:53–60.
[26] Kubisztal J, Budniok A. Study of the oxygen evolution reaction on nickel-based composite coatings in alkaline media. Int J Hydrogen Energy 2008;33:4488–94.
[27] Lee GJ, Zheng YC, Wu JJ. Fabrication of hierarchical bismuth oxyhalides (BiOX, X= Cl, Br, I) materials and application of photocatalytic hydrogen production from water splitting. Catal Today 2018;307:197–204.
[28] Wang M, Shen S, Li L, Tang Z, Yang J. Effects of sacrificial reagents on photocatalytic hydrogen evolution over different photocatalysts. J Mater Sci 2017;52:5155–64.
[29] Anila EI, Safeera TA, Reshmi R. Photoluminescence of nanocrystalline ZnS thin film grown by sol–gel method. J Fluoresc 2015;25:227–30.